Published in final edited form as:

Cancer Res. 2016 April 15; 76(8): 2231–2242. doi:10.1158/0008-5472.CAN-15-1538.

Immunoregulatory protein B7-H3 reprograms glucose metabolism in cancer cells by ROS-mediated stabilization of HIF-1α

Sangbin Lim[1,£], **Hao Liu**[1,2,£], **Luciana Madeira da Silva**[1,£], **Ritu Arora**[1], **Zixing Liu**[1], **Joshua B. Phillips**[1], **David C. Schmitt**[1], **Tung Vu**[1], **Steven McClellan**[1], **Yifeng Lin**[3], **Wensheng Lin**[3], **Gary A. Piazza**[1], **Oystein Fodstad**[1,4], and **Ming Tan**[1,5]

[1]Center for Cell Death and Metabolism, Mitchell Cancer Institute, University of South Alabama, Mobile, USA

[2]Department of Biochemistry & Molecular Biology, West China School of Preclinical and Forensic Medicine, Sichuan University, Chengdu, China

[3]Department of Neuroscience, University of Minnesota, Minneapolis, Minnesota, USA

[4]Department of Tumor Biology, Norwegian Radium Hospital, Oslo University Hospital, and Institute for Clinical Medicine, Faculty of Medicine, University of Oslo, Oslo, Norway

[5]Department of Biochemistry & Molecular Biology, University of South Alabama, Mobile, USA

Abstract

B7-H3 is a member of B7 family of immunoregulatory transmembrane glycoproteins expressed by T cells. While B7-H3 overexpression is associated with poor outcomes in multiple cancers, it is also has immune-independent roles outside T cells and its precise mechanistic contributions to cancer are unclear. In this study, we investigated the role of B7-H3 in metabolic reprogramming of cancer cells in vitro and in vivo. We found that B7-H3 promoted the Warburg effect, evidenced by increased glucose uptake and lactate production in B7-H3-expressing cells. B7-H3 also increased the protein levels of HIF-1α and its downstream targets, LDHA and PDK1, key enzymes in the glycolytic pathway. Further, B7-H3 promoted ROS-dependent stabilization of HIF-1α by suppressing the activity of the stress-activated transcription factor Nrf2 and its target genes, including the antioxidants SOD1, SOD2, and PRX3. Metabolic imaging of human breast cancer xenografts in mice confirmed that B7-H3 enhanced tumor glucose uptake and tumor growth. Together, our results illuminate the critical immune-independent contributions of B7-H3 to cancer metabolism, presenting a radically new perspective on B7 family immunoregulatory proteins in malignant progression.

Corresponding Authors: Hao Liu, Department of Biochemistry & Molecular Biology, West China School of Preclinical and Forensic Medicine, Sichuan University, Chengdu, China. Phone: 86-28-8550-2491; ; Email: liuhaoy@hotmail.com; Oystein Fodstad, Department of Tumor Biology, Institute for Cancer Research, Oslo, Norway. Phone: 47-229-359-37. ; Email: Oystein.Fodstad@rr-research.no; Ming Tan, Mitchell Cancer Institute, University of South Alabama, Mobile, USA. Phone: 251-460-6993; ; Email: mtan@health.southalabama.edu.

[£]These authors contributed equally to this work.

Conflict of interest statement: None of the authors have a conflict of interest to declare.

Keywords

B7-H3; B7H3; CD276; Glycolysis; Reactive Oxygen Species; HIF-1α

Introduction

B7-H3 is a glycoprotein that belongs to the B7 family of immunoregulatory proteins. B7-H3 is expressed in low levels in most normal tissues, but is overexpressed in a wide variety of cancers and is associated with tumor progression, metastasis and poor patient outcome (1). B7-H3 overexpression in breast cancer is highly prevalent, and is associated with positive lymph node metastasis and advanced disease (2,3). B7-H3 has recently been successfully used as a biomarker for ultrasound molecular imaging in breast cancer (4). Due to a large difference in expression between tumors and normal tissues, and its important function in cancer progression, B7-H3 has emerged as a promising new therapeutic target and biomarker for breast cancer, including triple negative breast cancer (2,3,5,6).

The predominant splicing variant of B7-H3 in humans is the 4Ig-B7-H3, which consists in exon duplication of the extracellular IgV-IgC domains followed by a transmembrane domain and a short cytoplasmic carboxy-tail with no conserved signaling motifs (7–10). In contrast, exon duplication does not occur in mice, which only express the 2Ig-B7-H3 isoform. In addition, a soluble B7-H3 splicing variant lacking the transmembrane domain has been found in peripheral blood mononuclear cells (11). Currently, there is a complex scenario for the immunomodulatory role of B7-H3 since both T-cell costimulatory and coinhibitory functions for human 4Ig-B7-H3 have been reported under different contexts (1). These conflicting functions are currently attributed to possible distinct B7-H3 receptors in target cells, but could also be explained by different functions of the various B7-H3 splicing isoforms, or differential glycosylation patterns of B7-H3. TLT-2 has been described as a co-receptor for murine B7-H3 in CD8(+) T cell activation, with a co-stimulatory function of the murine B7-H3/TLT-2 pathway (12). However, this result has not been confirmed by other studies and the identity of the binding partner(s) for human 4Ig-B7-H3 remains elusive (13–15).

Despite its controversial immunological role, the immune-independent functions of B7-H3 in cancer malignancy are almost unknown. We and others have shown that B7-H3 mediates breast cancer invasion, metastasis and drug resistance and that silencing B7-H3 delays tumor growth and sensitizes cancer cells to chemotherapeutic agents (16–21). Similar results have also been confirmed by other groups in pancreatic cancer (21,22), colorectal cancer (20), hepatocellular carcinoma (23) and melanoma (19,24). In addition, we and others have shown that B7-H3 overexpression in breast cancer, melanoma and osteosarcoma cells increases their metastatic potential (16,19,25). B7-H3 has been shown to regulate matrix metalloproteinase MMP-2, Stat3 and IL-8 secretion, and tissue inhibitors of metalloproteinases TIMP-1 and TIMP-2 (16,19, 25, 26). These results clearly show that, in addition to immune regulatory function, B7-H3 possess immune-independent functions which may also contribute to cancer progression.

Increased aerobic glycolysis in cancer cells, also known as the Warburg effect, is considered as one of the most fundamental metabolic alterations during malignant transformation (27). It has been well accepted that the dysregulated metabolic reprograming gives cancer cell advantage for proliferation and survival (28). Here we show for the first time that B7-H3 plays an important role in the regulation of cellular glucose metabolism. Given the important roles of B7-H3 in cancer tumorigenesis and progression, this study further demonstrates that B7-H3 may serve as an excellent therapeutic target for cancer treatment.

Materials and Methods

Cell lines, culture and transfection conditions

Cancer cell lines MDA-MB-231, MDA-MB-435, SKBR3 and MDA-MB-468 were purchased from ATCC three years ago. The cell lines have been tested and authenticated. On June 26, 2015, the cells were tested by analyses of 8 autosomal short tandem repeat (STR) loci and the gender identity locus amelogenin.

MDA-MB-231 TR33, MDA-MB-231 shB7-H3, MDA-MB-435 TR33, MDA-MB-435 shB7-H3 cells were described earlier (17). SKBR3 and MDA-MB-468 cells were infected with retroviral particles expressing B7-H3 or the puromycin resistance gene only (vector control). Cells were selected and maintained with DMEM/F12 medium supplemented with 10% FBS and 2μg/ml puromycin.

Control scrambled siRNA and a siRNA targeting human B7-H3 were purchased from Sigma-Aldrich. Transfection was performed using Lipofectamine 2000 (Life Technologies).

Hypoxic conditions described in the experiments were achieved by using a GasPak Pouch (BD Biosciences), which is capable of reducing the oxygen concentration to less than or equal to 1% (mean percentage: 0.7%); or by treating cells with 200 μM cobalt (II) chloride ($CoCl_2$) for 24 hrs.

Lactate production assay

Cells were seeded in 12-well plate overnight and then medium was aspirated and replaced with fresh complete medium. Hypoxia treatment was performed in the GasPack Pouch. Alternatively, hypoxia-mimicking conditions were achieved by replacing medium with complete medium containing 200 μM $CoCl_2$. After 24 h, conditioned medium in each well was collected and the amount of lactate was then determined using the Lactate assay Kit (Biovision).

Glucose uptake assay

The set up described above for the lactate production assay was also used for the measurement of glucose uptake, except that after 24 h the conditioned medium was collected and stored at −20°C until assayed. Glucose measurements were determined using the Amplex Red Glucose/Glucose Oxidase Assay Kit (Molecular Probes).

Extracellular acidification rate and oxygen consumption rate measurements

Cancer cells were evaluated using an Extracellular Flux Analyzer (XF24; Seahorse Biosciences). The day prior to the assays, cells were seeded in 24-well plates (40,000 cells/well). Mitochondrial metabolism was evaluated with the XF Cell Mito Stress Kit, and the glycolytic metabolism with the XF Glycolysis Stress kit.

For the Mito Cell Stress assay, prior to the assay, growth medium was replaced with serum-free XF Seahorse Assay Medium supplemented with 1mM sodium pyruvate and 25mM glucose, and then cells were incubated for 1h at 37°C in an incubator without CO_2. Cartridges equipped with oxygen- and pH-sensitive probes had been pre-incubated with calibration solution overnight at 37°C in an incubator without CO_2. At the time of measurement, cells were then placed in the XF24 Extracellular Flux Analyzer with cartridges of probes. Oxygen consumption rate (OCR) and extracellular acidification rate (ECAR) were evaluated in a time-course before and after injection of the following compounds: 1) oligomycin (1μM final concentration); 2) FCCP (Carbonyl cyanide-*4*-(trifluoromethoxy)phenylhydrazone; 0.75μM final concentration); 3) antimycin A + rotenone (1.5μM each final concentration). The Glycolysis Stress assay was performed in a similar fashion, but using XF Seahorse Glycolysis Stress Base Medium supplemented with 2mM L-glutamine, and injection of the following compounds: 1) glucose (10mM final concentration); 2) oligomycin (1μM final concentration); 3) 2-deoxyglucose (2-DG; 100mM final concentration).

Determination of intracellular ROS

Intracellular ROS were measured using CellROX deep red and MitoSOX red fluorogenic probes (Molecular Probes/Invitrogen). For hypoxic conditions, cells were placed in the BD GasPak pouch for 48 hours. Cells were harvested and placed in growth medium, loaded with 5 μM CellROX deep red and MitoSOX red for 15 minutes and then washed once with PBS. Fluorescence intensity was measured by flow-cytometry (BD LSR II-BD Bioscience).

Quantitative Real-Time PCR

Total RNA was isolated from cultured cells using TRIzol reagent (Life Technologies). DNase-treated total RNA were used in each cDNA synthesis reaction using the High-Capacity cDNA Reverse Transcription kit (Applied Biosystems). Quantitative PCR (qPCR) was performed with Fast Start Universal SYBR Green Master (Roche Life Science). Each qPCR reaction contained 5μl of diluted cDNA (5× dilution), 6.5μl nuclease-free distilled water, 12.5μl SYBR Green Master Mix, 0.5μl of each primer (5pmol/reaction). Sequences of primers: SOD2-fw (5' CTGGACAAACCTCAGCCCTA 3'), SOD2-rv (5' TGATGGCTTCCAGCAACTC 3'), Nrf2-fw (5' AGTGGATCTGCCAACTACTC 3'), Nrf2-rv (5' CATCTACAAACGGGAATGTCTG 3'). qPCR reactions were performed using the CFX96 Real-Time System with the C1000 Touch Thermal Cycler (BioRad) using the following protocol: 10 min at 95°C, followed by 50 cycles of 15s at 95°C and 1 min at 60°C, and finally a 65–95°C ramp to determine melting curve. The relative amounts of mRNA were calculated by using the comparative Ct method.

Mitochondria fractionation

The mitochondrial fraction and mitochondrial proteins were prepared using Qproteome Mitochondria Isolation Kit (Qiagen). Cells were washed with PBS and resuspended with Lysis buffer from Kit and then incubated at 4 °C for 10 min. Following a centrifugation at 1,000 × g at 4 °C for 10 min, the supernatant was separated from the pellet. The supernatant was stored at −20 °C for further investigation. The pellet was resuspended in ice-cold Disruption buffer and homogenized by using a 25G needle and a syringe. Following a centrifugation at 1,000 × g at 4 °C for 10 min, the supernatant was transferred to a new tube. The supernatant was centrifuged at 6,000 × g at 4 °C for 10 min. The pellet containing mitochondria was resuspended in protein lysis buffer and protein concentration was determined using the Bradford assay.

Nuclear fractionation

Cells were washed with PBS and resuspended in harvest buffer (10mM HEPES pH 7.9, 50mM NaCl, 0.5M Sucrose, 0.1mM EDTA and 0.5% Triton X100). The supernatant was incubated on ice for 5 min. Following a centrifugation at 100 × g at 4 °C for 10 min, the supernatant was separated from the pellet. The pellet was washed twice in Buffer A (10mM HEPES pH 7.9, 10mM KCl, 0.1mM EDTA and 0.1mM EGTA). Following a centrifugation at 3,000 × g at 4 °C for 10 min, the pellet was resuspended in Buffer C (10mM HEPES pH 7.9, 0.5M NaCl, 0.1mM EDTA, 0.1mM EGTA and 0.1% NP40). The nuclear pellet was collected by centrifugation at 13,000 × g at 4 °C for 10 min and ressuspended in protein lysis buffer.

Western blot analysis

Western blotting was performed as we previously reported (17). Anti-human B7-H3 (AF1027) antibody was purchased from R&D Systems; anti-HIF-1α (#610959) was from BD Biosciences; anti-human B7-H3 (sc-376769), anti-Nrf2 (sc-722), anti-SOD1 (sc-11407), anti-SOD2 (sc-30080), anti-Prx3 (sc-59661), anti-α-tubulin (sc-23948) and anti-VDAC (sc-58649) were from Santa Cruz; anti-lamin B1 (MA1–06103) and anti-mtHSP70 (MA3–028) were from Thermo Scientific; anti-β-actin (#3700), anti-survivin (#2808), anti-LDHA (#2012) were from Cell signaling; anti-PDK1 (ADI-KAP-PK112) was from Enzo Life Sciences.

Animal tumor xenograft studies

Mouse experiments were done in accordance with protocols approved by the Institutional Animal Care and Use Committees of University of South Alabama. Six-week-old female athymic nude mice were used in the experiments. 1×10^6 cancer cells suspended in 200 μL of PBS and matrigel mixture (1:1) were injected into the mammary fat pads of each mouse. After development of palpable tumors, diameter of each tumor was measured every week using digital micrometer calipers, and the tumor volume was calculated using the formula: volume (mm^3) = $W^2 \times L/2$, where W and L are the minor and major diameters, respectively.

Glucose uptake analysis via fluorescent imaging *in vivo*

Five weeks after the cell injection, the mice were injected intravenously with 10nmoles / 100uL of XenoLight RediJect 2-DeoxyGlucosone (DG)-750 (XenoLight, Perkin Elmer). After 24 hrs of dye injection the mice were analyzed for glucose uptake by fluorescent imaging using an IVIS-200 camera system (Xenogen) (10). Ten minutes before *in vivo* imaging, mice were anesthetized with 3% isofurane using the XGI-8 Gas Anesthesia System (Caliper Life Sciences). The imaging results were analyzed using Living Image software. A region of interest was manually selected over relevant regions of signal intensity, and the intensity was recorded as the efficiency. Fluorescent intensity obtained from each mouse was plotted using Graph Pad Prism software version 5.0.

Statistical analysis

Statistical significance for experimental data was determined with unpaired student's *t*-test (GraphPad Prism). Statistical differences of $P<0.05$ were considered significant.

Results

B7-H3 promotes the Warburg effect in cancer cells

To study the possible role of B7-H3 in the regulation of glucose metabolism in cancer cells, we used two stable B7-H3 knockdown cell variants derived from the breast cancer cell line MDA-MB-231 and the melanoma cell line MDA-MB-435 that we described previously (17). Effective knockdown of B7-H3 expression was confirmed (Fig. 1A; TR33 denotes scramble vector control).

We measured lactate production and glucose uptake, two hallmarks of glycolysis, in control and B7-H3 knockdown cells. Both MDA-MB-231 shB7-H3 and MDA-MB-435 shB7-H3 cells showed a significantly lower lactate production (Fig. 1B) and glucose uptake (Fig. 1C) than their respective scramble control cells, both in normoxia and hypoxia conditions. As expected, all cells grown under hypoxia showed a higher rate of glycolysis compared with the cells grown in normoxia. We also obtained the similar results from cells treated with $CoCl_2$, which mimics hypoxia conditions by preventing HIF hydroxylation (Fig. S1, A and B). These results indicate that B7-H3 expression promotes glycolysis in these cancer cells.

To further characterize the role of B7-H3 in cancer cell glucose metabolism, we used the XF24 to measure in real-time the OCR and the ECAR as indicatives of oxidative respiration and glycolysis, respectively, in various breast cancer cell lines with stable B7-H3 knockdown or overexpression. We used the Mito Cell Stress and the Glycolysis Stress assays to determine various parameters of mitochondrial respiration and glycolytic capacity of the cells. We found that knockdown B7-H3 in MDA-MB-231 cells decreased basal ECAR (Fig. 2, C and F) and increased basal OCR (Fig. 2A) when compared to control cells (TR33), which resulted in an increased basal OCR/ECAR ratio (Fig. 2G) that is indicative of an anti-Warburg effect. Both glycolysis and glycolytic reserve capacity are decreased in MDA-MB-231 shB7-H3 cells when compared to control cells (Fig. 2, C and E). Conversely, overexpression of B7-H3 in SKBR3 breast cancer cells decreased basal OCR (Fig. 2B) and increased basal ECAR (Fig. 2D) when compared to empty vector (EV) control cells.

Strikingly, overexpression of B7-H3 significantly increased both glycolysis and glycolytic reserve in SKBR3 cells (Fig. 2, D and H). Similarly, B7-H3 overexpression in MDA-MB-468 breast cancer cells also increased basal ECAR (Fig. 2I) and decreased the basal OCR/ECAR ratio (Fig. 2J), indicating that B7-H3 overexpression promotes the Warburg effect in breast cancer cells.

We next tested whether B7-H3 knockdown cells respond differently to glycolysis inhibition compared to the control cells. We treated MDA-MB-231 and MDA-MB-435 shB7-H3 cells and their control cells with a specific glycolysis inhibitor oxamate, a pyruvate analog that directly inhibits the conversion of pyruvate to lactate by lactate dehydrogenase, and then examined its effect on cell growth. The results showed that oxamate greatly inhibited the growth of all the cells in a dose-dependent manner (Fig. S2A). However, compared to control cells, the growth of B7-H3 knockdown cells MDA-MB-231 shB7-H3 and MDA-MB-435 shB7-H3 was less inhibited, indicating B7-H3 high-expressing cells are more sensitive to glycolysis inhibition. These results were further confirmed by colony formation assay with B7-H3 high and low-expressing cells (Fig. S2B). To further test this, we compared the growth of these cells in medium with or without glucose (Fig. S3A). Although glucose depletion slowed the growth of all tested cells when compared to complete media controls, the growth of both 231 shB7-H3 and 435 shB7-H3 cells was less inhibited by glucose depletion than that of their control counterparts. This indicates that B7-H3 knockdown cells are less sensitive to glucose deprivation as compared to control cells. To further confirm whether B7-H3 increased growth rate required aerobic glycolysis, we grew cells in media containing galactose instead of glucose, thereby reducing glycolytic flux and forcing the cells to rely on mitochondrial oxidative phosphorylation. Under these conditions, B7-H3 knockdown cells grew at the almost same rate as control vector cells (Fig. S3B), demonstrating that the increased proliferation of B7-H3 expressing cells required enhanced glucose metabolism. Taken together, these results suggested B7-H3 play an important role in reprogramming cancer cell metabolism in favor of glycolysis, and as a result, promoting cell growth.

B7-H3 regulates glycolysis through HIF-1α

HIF-1α functions as a master regulator in the reprogramming of cancer metabolism in favor of glycolysis. To test whether B7-H3 promotes glycolysis in cancer cells involves HIF-1α, we first investigated whether B7-H3 regulates HIF-1α protein level. The western-blot analysis revealed HIF-1α protein level was decreased in B7-H3 knockdown cells compared to their control cells in both normoxia and hypoxia conditions (Fig. 3A). We further confirmed these results in MDA-MB-231 by transiently knockdown B7-H3 using a siRNA that targets a different sequence than that in the shB7-H3 construct (Fig. S4). Importantly, HIF-1α level was rescued in MDA-MB-231 shB7-H3 cells transiently transfected with a B7-H3 expression vector (Fig. 3B). We next, evaluated the levels of two direct targets of HIF-1α, lactate dehydrogenase A (LDHA) and pyruvate dehydrogenase kinase 1 (PDK1), and found that both are downregulated in B7-H3 knockdown cells under both normoxia and hypoxia conditions when compared to control cells (Fig. 3C). Conversely, overexpression of B7-H3 in SKBR3 and MDA-MB-468 cells results in increased levels of HIF-1α, LDHA and PDK1 under hypoxia conditions (Fig. 3, D–E). Altogether, these results show that the B7-

H3-induced metabolic shift in cancer cells is mediated by HIF-1α and its targets in the glycolytic pathway.

Regulation of HIF-1α stability by B7-H3 is ROS-dependent

We next investigated how B7-H3 regulates HIF-1α. Since we did not detect obvious changes in HIF-1α mRNA levels between B7-H3 knockdown cells and control cells (Fig. S5), we checked whether B7-H3 regulates HIF-1α protein stability. After treatment with the proteasome inhibitor MG132, HIF-1α protein was induced to the similar level in B7-H3 knockdown cells as in the control cells, indicating that B7-H3 upregulates HIF-1α through protein stabilization (Fig. 4A).

Reactive oxygen species (ROS) have been shown to inhibit the prolyl hydroxylases (PHDs) and stabilize HIF-1α, thus we tested whether stabilization of HIF-1α by B7-H3 is ROS-dependent. We measured cellular ROS levels under hypoxia condition by staining with CellROX deep red (Fig. 4B) and MitoSOX red (Fig. 4C) and measuring fluorescence levels by flow-cytometry. Knockdown of B7-H3 in MDA-MB-231 and MDA-MB-435 cells results in lower levels of ROS when compared to control cells (Fig. 4, B and C). Conversely, overexpression of B7-H3 in MDA-MB-468 cells results in higher ROS levels than in control cells (Fig. 4, B and C). After treatment of NAC and PEG-catalase, ROS levels were reduced (Fig. S6). These results show that B7-H3 regulates ROS levels in cancer cells.

Next, we tested whether suppressing ROS could block the stabilization of HIF-1α by B7-H3. Indeed, treatment with the ROS scavenger N-acetylcysteine (NAC) and PEG-catalase under hypoxia reduced HIF-1α protein (Fig. 4, D and E). Accordingly, suppressing ROS also reduced LDHA and PDK1 in control cells to the similar levels as in B7-H3 knockdown cells (data not shown). Pentose phosphate pathway (PPP) is important in regeneration of NADPH from $NADP^+$. NADPH is required for the scavenging of ROS. Therefore, the PPP plays a pivotal role in helping glycolytic cancer cells to suppress oxidative stress. We thus examined the activity of G6PD, a critical enzyme in PPP, in B7-H3 knock-down and overexpressing cells. The results showed that B7-H3 expression increased G6PD activity under hypoxia (Fig. S7A), indicating that in addition to promoting glycolysis, B7-H3 expression also increases PPP to combat ROS. Finally, to test whether decreased ROS could underlie the reduced proliferation of B7-H3 knockdown cells, we cultured cells with NAC and measured growth rates. Strikingly, we found that B7-H3 knockdown cells grew at the almost same rate as control cells after treated with NAC (Fig. S8). Thus, regulation of ROS by B7-H3 plays an important role in upregulation of HIF-1α and cell growth in B7-H3 expressing cells.

B7-H3 regulates ROS level through Nrf2 and its targeting antioxidant enzymes

To investigate how B7-H3 regulates ROS, we evaluated the levels of antioxidant enzymes in isolated mitochondria from cancer cells with different expression levels of B7-H3. Interestingly, we found that B7-H3 high expression was inversely correlated to the mitochondrial superoxide dismutase 2 (SOD2) and peroxiredoxin 3 (Prx3) in both MDA-MB-231 shB7-H3 knockdown and SKBR3 B7-H3 overexpression cells (Fig. 5A). In addition, we monitored the expression of superoxide dismutase 1 (SOD1), a cytoplasmic enzyme that can translocate to the mitochondrial intermembrane space, and found that,

although cytoplasmic SOD1 was not altered either in SKBR3 B7-H3 or in MDA-MB-231 shB7-H3 cells, mitochondrial SOD1 was decreased in SKBR3 B7-H3 cells (Fig. 5A). Moreover, knockdown B7-H3 increased the enzyme activity of mitochondrial SOD, while the mitochondrial SOD activity was decreased in B7-H3 high overexpression cells (Fig. S6, B and C). These results indicated that B7-H3 regulates the mitochondrial antioxidant enzymes SOD1, SOD2, and Prx3. Because these antioxidant enzymes are target molecules of the transcriptional factor Nrf2, we examined the nuclear translocation of Nrf2, which is an indicator of Nrf2 activation, in MDA-MB-231 shB7-H3 knockdown and SKBR3 and MDA-MB-468 B7-H3 overexpressing cells. The results showed that B7-H3 expression suppresses Nrf2 translocation into the nucleus (Fig. 5B). Finally, we monitored mRNA levels of Nrf2 target gene SOD2 and found that it was also inversely correlated with B7-H3 expression in MDA-MB-231 shB7-H3 knockdown cells and SKBR3 B7-H3 overexpression cells when compared to their respective control cells (Fig. 5, C–D). These results indicated that B7-H3 regulates cellular ROS level through Nrf2 and its targeting antioxidant enzymes.

B7-H3 promotes glucose uptake and tumor growth in breast tumor xenografts

To examine whether B7-H3 promotes glucose uptake and tumor growth in a mouse model, we used the overexpression model of B7-H3 in MDA-MB-468 human breast cancer cells to monitor tumor growth and glucose uptake *in vivo*. XenoLight RediJect 2-DeoxyGlucosone (DG)-750, a fluorescent probe that contains four molecules of 2-deoxyglucose (2-DG) per dye molecule was used to visualize the tumor size and the rate of glucose uptake by tumors. B7-H3 overexpressing MDA-MB-468 cells grew significantly larger tumors in comparison to control cells (Fig. 6, A–C). Moreover, we observed a significant increase in glucose uptake by B7-H3 overexpressing tumors when compared to vector controls (Fig. 6, D–E). To further confirm our results, we also examined the tumor growth and glucose uptake *in vivo* with MDA-MB-231 shB7-H3 knockdown xenograft mouse model. As expected, knockdown of B7-H3 resulted in significantly smaller tumors when compared to scramble controls (Fig. 6, F–H) and decreased glucose uptake by tumors (Fig. 6, I–J). Furthermore, downregulation of HIF-1α, LDHA and PDK1 in MDA-MB-231 shB7-H3 tumor in comparison to vector control tumor was confirmed by immunohistochemistry analysis of xenograft tumors (Fig. S9). Altogether, both of our two independent xenograft mouse models support our *in vitro* findings showing that B7-H3 plays a critical role in reprogramming glucose metabolism by enhancing aerobic glycolysis.

Discussion

Although most functional studies focus on the immunological role of B7-H3, our previous studies have revealed that B7-H3 has autocrine cellular functions in cancer cells that affect tumor progression (16,17,19). Here we demonstrated that B7-H3 regulates glucose metabolism through ROS mediated HIF-1α stabilization, which contributes to B7-H3 enhanced tumor growth (Figure 7). We showed that knockdown of B7-H3 inhibits glycolysis by the decreased the stability and activity of HIF-1α, as well as its downstream targets LDHA and PDK1. Conversely, overexpression of B7-H3 showed a reverse effect. Moreover, B7-H3 promotes HIF-1α stability via increased ROS by suppressing the activity of transcription factor Nrf2 and Nrf2 target genes. Furthermore, in two independent xenograft

mouse models we showed that B7-H3 promotes breast cancer uptake of glucose and tumor growth *in vivo*. These novel findings provide a new insight for the role of B7-H3 in cellular metabolic reprogramming of cancer cells.

HIF-1α plays a central role as integrator of pathways involved in glycolysis (29). Our results revealed that knockdown of B7-H3 downregulates HIF-1α and its direct targets, LDHA and PDK1. Conversely, overexpression of B7-H3 increases HIF-1α, LDHA and PDK1. Both LDHA and PDK1 play a critical role in glycolysis. Thus we demonstrate that HIF-1α plays a central role in the regulation of glycolysis by B7-H3.

To study how B7-H3 regulates HIF-1α stability, we found that ROS levels were significantly increased in B7-H3 overexpressing cells and conversely decreased in B7-H3 knockdown cells. Several studies have shown that ROS are both necessary and sufficient to stabilize and activate HIF-1α (29). Here we showed that the ROS scavengers reduced HIF-1α, as well as the cell proliferative rate, to almost the similar levels in B7-H3 expressing and knockdown cells. We revealed that B7-H3 expression reduced Nrf2 activity, resulting in downregulation of the Nrf2 antioxidant targets SOD1, SOD2, and Prx3 (30–32). However, the lack of knowledge of B7-H3 receptors and/or binding partners leaves the mechanism linking B7-H3 to Nrf2 and antioxidant enzymes to be still elucidated.

Our findings on the role of B7-H3 in cellular glucose metabolism discover a novel biological function of the B7 family proteins, which could provide an opportunity for cancer therapeutic intervention. Currently, phase I clinical trials have been testing the safety of the anti-B7-H3 antibody 8H9 and MGA271 in several types of cancers (5,33,34). However, both antibodies have only been deployed as a tumor-targeting agents and it is unknown whether they can also affect the intrinsic functions of B7-H3. Our studies indicate that therapeutic agents designed for inhibiting the intrinsic tumor promoting function of B7-H3 is promising for cancer treatment.

Based on evidence that we present here, it is tempting to hypothesize that B7-H3 might also favor tumor growth by manipulating cancer immunosurveillance through alterations in the metabolism of cancer cells and immune cells. Numerous reports demonstrated that differentiation and activation of distinct subsets of immune cells are tightly modulated by specific metabolic programs (35–37). Murine B7-H3 has been reported suppressing Th1 effector responses (38,39). In addition, Tregs upregulate B7-H3 expression in dendritic cells (DC) upon contact, subsequently inducing immunossupressive functions of DCs (40). Tumor infiltration with Tregs (Foxp3+ T cells) is associated with suppression of antitumor immunity and has been associated with worse prognosis in cancer patients (41,42). Interestingly, a recent study of breast cancer patients revealed that B7-H3 high/Foxp3 high tumor staining was associated with significantly shorter recurrence-free survival than that of B7-H3 low/Foxp3 low (43). Future studies should investigate whether B7-H3-induced metabolic reprogramming also plays a role in regulation of cancer immunity to favor tumor growth and metastasis.

Supplementary Material

Refer to Web version on PubMed Central for supplementary material.

Acknowledgments

We are grateful to the support from The Vincent F. Kilborn, Jr. Cancer Research Foundation (M. Tan), National Institutes of Health Grants R01CA149646 (M. Tan) and R01NS073132 (W. Lin). The Radiumhospitalets Legater Project 334003 (M. Tan and O. Fodstad) and National Natural Science Foundation of China Project 81201559 (H. Liu).

References

1. Wang L, Kang FB, Shan BE. B7-H3-mediated tumor immunology: Friend or foe? Int J Cancer. 2014; 134(12):2764–2771. [PubMed: 24013874]
2. Arigami T, Narita N, Mizuno R, Nguyen L, Ye X, Chung A, et al. B7-h3 ligand expression by primary breast cancer and associated with regional nodal metastasis. Ann Surg. 2010; 252(6):1044–1051. [PubMed: 21107115]
3. Liu C, Liu J, Wang J, Liu Y, Zhang F, Lin W, et al. B7-H3 expression in ductal and lobular breast cancer and its association with IL-10. Mol Med Rep. 2013; 7(1):134–138. [PubMed: 23128494]
4. Bachawal SV, Jensen KC, Wilson KE, Tain L, Lutz AM, Willmann JK. Breast cancer detection by B7-H3 targeted ultrasound molecular imaging. Cancer Res. 2015
5. Loo D, Alderson RF, Chen FZ, Huang L, Zhang W, Gorlatov S, et al. Development of an Fc-enhanced anti-B7-H3 monoclonal antibody with potent antitumor activity. Clin Cancer Res. 2012; 18(14):3834–3845. [PubMed: 22615450]
6. Kraan J, van den Broek P, Verhoef C, Grunhagen DJ, Taal W, Gratama JW, et al. Endothelial CD276 (B7-H3) expression is increased in human malignancies and distinguishes between normal and tumour-derived circulating endothelial cells. Br J Cancer. 2014; 111(1):149–156. [PubMed: 24892449]
7. Ling V, Wu PW, Spaulding V, Kieleczawa J, Luxenberg D, Carreno BM, et al. Duplication of primate and rodent B7-H3 immunoglobulin V- and C-like domains: divergent history of functional redundancy and exon loss. Genomics. 2003; 82(3):365–377. [PubMed: 12906861]
8. Zhou YH, Chen YJ, Ma ZY, Xu L, Wang Q, Zhang GB, et al. 4IgB7-H3 is the major isoform expressed on immunocytes as well as malignant cells. Tissue Antigens. 2007; 70(2):96–104. [PubMed: 17610414]
9. Steinberger P, Majdic O, Derdak SV, Pfistershammer K, Kirchberger S, Klauser C, et al. Molecular characterization of human 4Ig-B7-H3, a member of the B7 family with four Ig-like domains. J Immunol. 2004; 172(4):2352–2359. [PubMed: 14764704]
10. Sun M, Richards S, Prasad DV, Mai XM, Rudensky A, Dong C. Characterization of mouse and human B7-H3 genes. J Immunol. 2002; 168(12):6294–6297. [PubMed: 12055244]
11. Chen W, Liu P, Wang Y, Nie W, Li Z, Xu W, et al. Characterization of a soluble B7-H3 (sB7-H3) spliced from the intron and analysis of sB7-H3 in the sera of patients with hepatocellular carcinoma. PLoS One. 2013; 8(10):e76965. [PubMed: 24194851]
12. Hashiguchi M, Kobori H, Ritprajak P, Kamimura Y, Kozono H, Azuma M. Triggering receptor expressed on myeloid cell-like transcript 2 (TLT-2) is a counter-receptor for B7-H3 and enhances T cell responses. Proc Natl Acad Sci U S A. 2008; 105(30):10495–10500. [PubMed: 18650384]
13. Leitner J, Klauser C, Pickl WF, Stockl J, Majdic O, Bardet AF, et al. B7-H3 is a potent inhibitor of human T-cell activation: No evidence for B7-H3 and TREML2 interaction. Eur J Immunol. 2009; 39(7):1754–1764. [PubMed: 19544488]
14. Vigdorovich V, Ramagopal UA, Lazar-Molnar E, Sylvestre E, Lee JS, Hofmeyer KA, et al. Structure and T cell inhibition properties of B7 family member, B7-H3. Structure. 2013; 21(5): 707–717. [PubMed: 23583036]

15. Yan R, Yang S, Gu A, Zhan F, He C, Qin C, et al. Murine b7-h3 is a co-stimulatory molecule for T cell activation. Monoclon Antib Immunodiagn Immunother. 2013; 32(6):395–398. [PubMed: 24328742]
16. Chen YW, Tekle C, Fodstad O. The immunoregulatory protein human B7H3 is a tumor-associated antigen that regulates tumor cell migration and invasion. Curr Cancer Drug Targets. 2008; 8(5): 404–413. [PubMed: 18690846]
17. Liu H, Tekle C, Chen YW, Kristian A, Zhao Y, Zhou M, et al. B7-H3 silencing increases paclitaxel sensitivity by abrogating Jak2/Stat3 phosphorylation. Mol Cancer Ther. 2011; 10(6):960–971. [PubMed: 21518725]
18. Nygren MK, Tekle C, Ingebrigtsen VA, Fodstad O. B7-H3 and its relevance in cancer; immunological and non-immunological perspectives. Front Biosci (Elite Ed). 2011; 3:989–993. [PubMed: 21622107]
19. Tekle C, Nygren MK, Chen YW, Dybsjord I, Nesland JM, Maelandsmo GM, et al. B7-H3 contributes to the metastatic capacity of melanoma cells by modulation of known metastasis-associated genes. Int J Cancer. 2012; 130(10):2282–2290. [PubMed: 21671471]
20. Zhang T, Jiang B, Zou ST, Liu F, Hua D. Overexpression of B7-H3 augments anti-apoptosis of colorectal cancer cells by Jak2-STAT3. World J Gastroenterol. 2015; 21(6):1804–1813. [PubMed: 25684945]
21. Zhao X, Zhang GB, Gan WJ, Xiong F, Li Z, Zhao H, et al. Silencing of B7-H3 increases gemcitabine sensitivity by promoting apoptosis in pancreatic carcinoma. Oncol Lett. 2013; 5(3): 805–812. [PubMed: 23426281]
22. Zhao X, Li DC, Zhu XG, Gan WJ, Li Z, Xiong F, et al. B7-H3 overexpression in pancreatic cancer promotes tumor progression. Int J Mol Med. 2013; 31(2):283–291. [PubMed: 23242015]
23. Kang FB, Wang L, Li D, Zhang YG, Sun DX. Hepatocellular carcinomas promote tumor-associated macrophage M2-polarization via increased B7-H3 expression. Oncol Rep. 2015; 33(1): 274–282. [PubMed: 25370943]
24. Wang J, Chong KK, Nakamura Y, Nguyen L, Huang SK, Kuo C, et al. B7-H3 associated with tumor progression and epigenetic regulatory activity in cutaneous melanoma. J Invest Dermatol. 2013; 133(8):2050–2058. [PubMed: 23474948]
25. Wang L, Zhang Q, Chen W, Shan B, Ding Y, Zhang G, et al. B7-H3 is overexpressed in patients suffering osteosarcoma and associated with tumor aggressiveness and metastasis. PLoS One. 2013; 8(8):e70689. [PubMed: 23940627]
26. Xu L, Ding X, Tan H, Qian J. Correlation between B7-H3 expression and matrix metalloproteinases 2 expression in pancreatic cancer. Cancer Cell Int. 2013; 13(1):81. [PubMed: 23947693]
27. DeBerardinis RJ, Lum JJ, Hatzivassiliou G, Thompson CB. The biology of cancer: metabolic reprogramming fuels cell growth and proliferation. Cell metabolism. 2008; 7(1):11–20. [PubMed: 18177721]
28. Zhao Y, Butler EB, Tan M. Targeting cellular metabolism to improve cancer therapeutics. Cell death & disease. 2013; 4:e532. [PubMed: 23470539]
29. Semenza GL. HIF-1 mediates metabolic responses to intratumoral hypoxia and oncogenic mutations. J Clin Invest. 2013; 123(9):3664–3671. [PubMed: 23999440]
30. Bae SH, Sung SH, Lee HE, Kang HT, Lee SK, Oh SY, et al. Peroxiredoxin III and sulfiredoxin together protect mice from pyrazole-induced oxidative liver injury. Antioxid Redox Signal. 2012; 17(10):1351–1361. [PubMed: 22490042]
31. Dong J, Sulik KK, Chen SY. Nrf2-mediated transcriptional induction of antioxidant response in mouse embryos exposed to ethanol in vivo: implications for the prevention of fetal alcohol spectrum disorders. Antioxid Redox Signal. 2008; 10(12):2023–2033. [PubMed: 18759561]
32. Moon EJ, Giaccia A. Dual roles of NRF2 in tumor prevention and progression: possible implications in cancer treatment. Free Radic Biol Med. 2015; 79:292–299. [PubMed: 25458917]
33. Luther N, Zhou Z, Zanzonico P, Cheung NK, Humm J, Edgar MA, et al. The potential of theragnostic (1)(2)(4)I-8H9 convection-enhanced delivery in diffuse intrinsic pontine glioma. Neuro Oncol. 2014; 16(6):800–806. [PubMed: 24526309]

34. Modak S, Guo HF, Humm JL, Smith-Jones PM, Larson SM, Cheung NK. Radioimmunotargeting of human rhabdomyosarcoma using monoclonal antibody 8H9. Cancer Biother Radiopharm. 2005; 20(5):534–546. [PubMed: 16248769]

35. Gerriets VA, Rathmell JC. Metabolic pathways in T cell fate and function. Trends Immunol. 2012; 33(4):168–173. [PubMed: 22342741]

36. Kareva I, Hahnfeldt P. The emerging "hallmarks" of metabolic reprogramming and immune evasion: distinct or linked? Cancer Res. 2013; 73(9):2737–2742. [PubMed: 23423980]

37. Palsson-McDermott EM, O'Neill LA. The Warburg effect then and now: from cancer to inflammatory diseases. Bioessays. 2013; 35(11):965–973. [PubMed: 24115022]

38. Suh WK, Gajewska BU, Okada H, Gronski MA, Bertram EM, Dawicki W, et al. The B7 family member B7-H3 preferentially down-regulates T helper type 1-mediated immune responses. Nat Immunol. 2003; 4(9):899–906. [PubMed: 12925852]

39. Ueno T, Yeung MY, McGrath M, Yang S, Zaman N, Snawder B, et al. Intact B7-H3 signaling promotes allograft prolongation through preferential suppression of Th1 effector responses. Eur J Immunol. 2012; 42(9):2343–2353. [PubMed: 22733595]

40. Mahnke K, Ring S, Johnson TS, Schallenberg S, Schonfeld K, Storn V, et al. Induction of immunosuppressive functions of dendritic cells in vivo by CD4+CD25+ regulatory T cells: role of B7-H3 expression and antigen presentation. Eur J Immunol. 2007; 37(8):2117–2126. [PubMed: 17615586]

41. Bates GJ, Fox SB, Han C, Leek RD, Garcia JF, Harris AL, et al. Quantification of regulatory T cells enables the identification of high-risk breast cancer patients and those at risk of late relapse. J Clin Oncol. 2006; 24(34):5373–5380. [PubMed: 17135638]

42. Merlo A, Casalini P, Carcangiu ML, Malventano C, Triulzi T, Menard S, et al. FOXP3 expression and overall survival in breast cancer. J Clin Oncol. 2009; 27(11):1746–1752. [PubMed: 19255331]

43. Maeda N, Yoshimura K, Yamamoto S, Kuramasu A, Inoue M, Suzuki N, et al. Expression of B7-H3, a potential factor of tumor immune evasion in combination with the number of regulatory T cells, affects against recurrence-free survival in breast cancer patients. Ann Surg Oncol. 2014; 21(Suppl 4):S546–S554. [PubMed: 24562936]

44. Cai H, Peng F. 2-NBDG fluorescence imaging of hypermetabolic circulating tumor cells in mouse xenograft model of breast cancer. J Fluoresc. 2013; 23(1):213–220. [PubMed: 23054302]

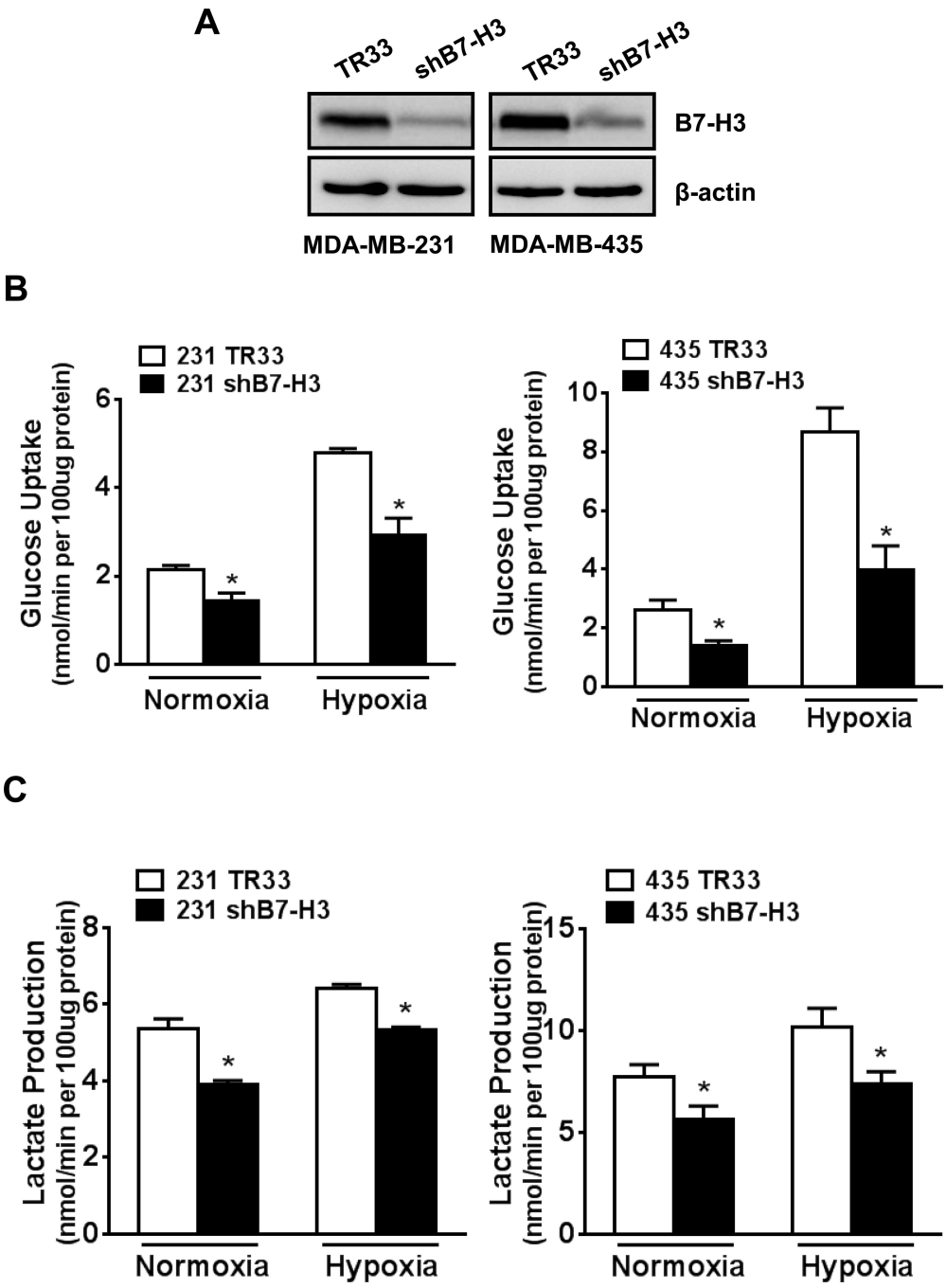

Figure 1. B7-H3 knockdown reduces glucose uptake and lactate production in breast cancer cells

(A) Western-blotting to validate knockdown of B7-H3 in two stable breast cancer cell lines, MDA-MB-231 and MDA-MB-435, which were generated by transfection with shRNA plasmids and puromycin selection (TR33, scramble vector control). (B) Glucose uptake and (C) lactate production were measured in B7-H3 knockdown cells grown in normoxia or hypoxia conditions for 24h.

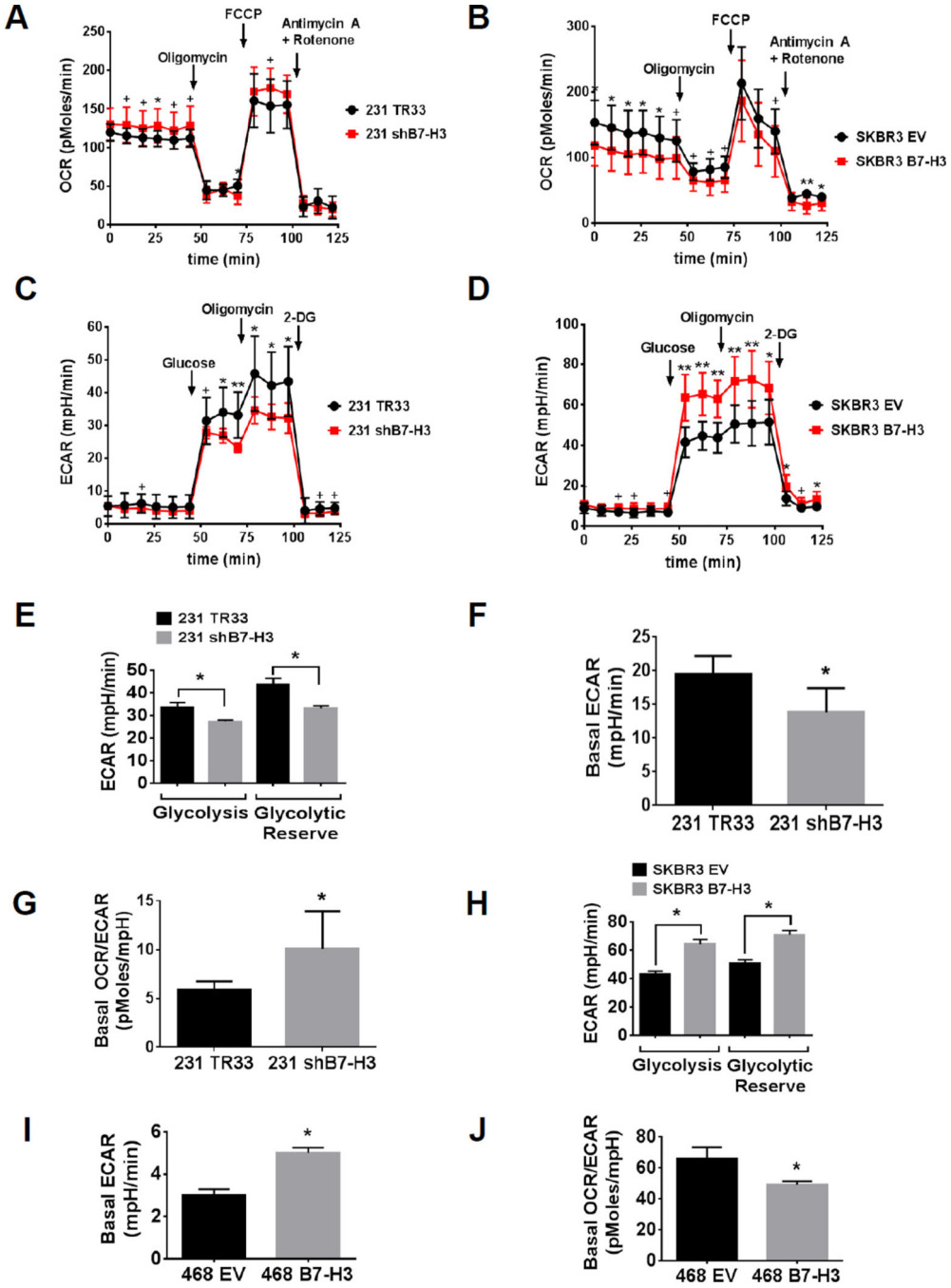

Figure 2. High B7-H3 expression increases extracellular acidification of the medium and decreases oxygen consumption rate in breast cancer cells

(A–D) Seahorse extracellular flux analyzer measurements of OCR (A–B) and ECAR (C–D) metabolic profile using the Mito Stress Cell (A–B) and Glycolysis Stress (C–D) assays in (A, C) MDA-MB-231 shB7-H3 knockdown or (B, D) SKBR3 B7-H3 overexpression breast cancer cells (TR33, scramble control vector for knockdown cells; EV, empty vector control for overexpression cells). Traces shown are representative of two independent experiments in which each data point represents replicates of five wells each ± SD (*p<0.05; +p<0.01; **p<0.001). (E, H) Bar graphs representing glycolysis (glucose-induced ECAR) and

glycolytic reserve (2-DG-induced ECAR subtracted of glucose-induced ECAR) were extracted from Glycolysis Stress assay results with (E) MDA-MB-231 shB7-H3 knockdown or (H) SKBR3 B7-H3 overexpression breast cancer cells. Glycolysis and glycolytic reserve were calculated using the average (±SD, $p<0.05$) of five replicate wells from one single data point that showed maximum response to addition of glucose or 2-DG, respectively. (F, G, I, J) Basal ECAR and OCR/ECAR rates were calculated using the average of three data points collected for each cell line in baseline measurements of the Mito Stress Cell assay, ±SD (*$p<0.05$). (F,G) MDA-MB-231 shB7-H3 knockdown or (I, J) MDA-MB-468 B7-H3 overexpression breast cancer cells.

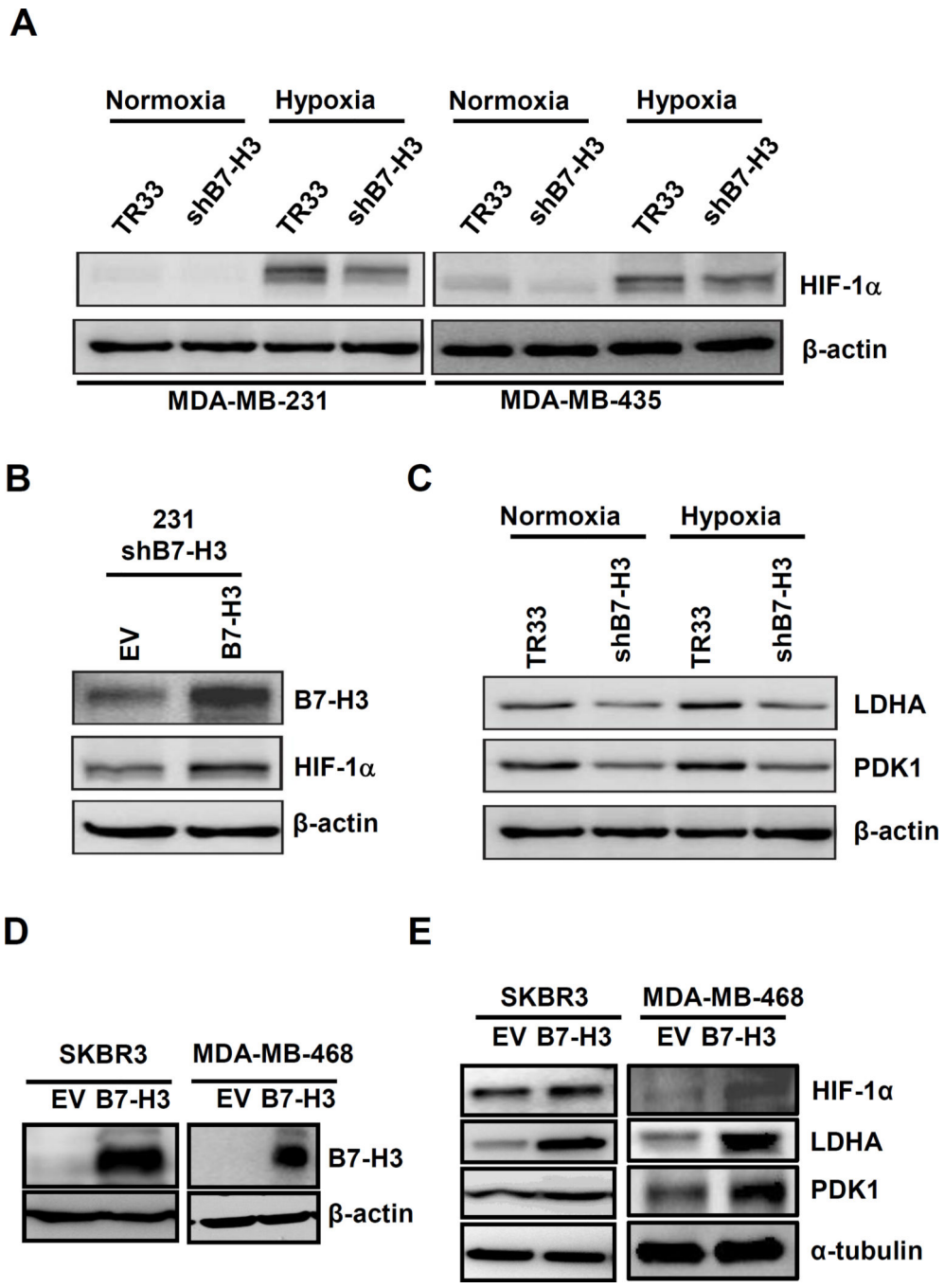

Figure 3. High B7-H3 expression increases protein levels of HIF-1α and its downstream targets, LDHA and PDK1

(A) Western-blot results of MDA-MB-231 (left panel) and MDA-MB-435 (right) shB7-H3 knockdown cells grown in normoxia or hypoxia conditions for 24h. (B) Transfection of MDA-MB-231 shB7-H3 cells with a B7-H3 expression construct to rescue B7-H3 increases HIF-1α protein levels. Twenty-four hours post-transfection, cells were transferred to GasPak pouches and incubated for additional 24h. (C) Western-blotting of MDA-MB-231 TR33 and shB7-H3 grown in normoxia or hypoxia conditions for 24h to monitor expression levels of LDHA and PDK1. (D) Expression levels of B7-H3 in two stable B7-H3 overexpressing

breast cell lines, SKBR3 and MDA-MB-468. (E) B7-H3 overexpression increases levels of HIF-1α, LDHA and PDK1 in SKBR3 and MDA-MB-468 cells grown in hypoxia conditions for 24h.

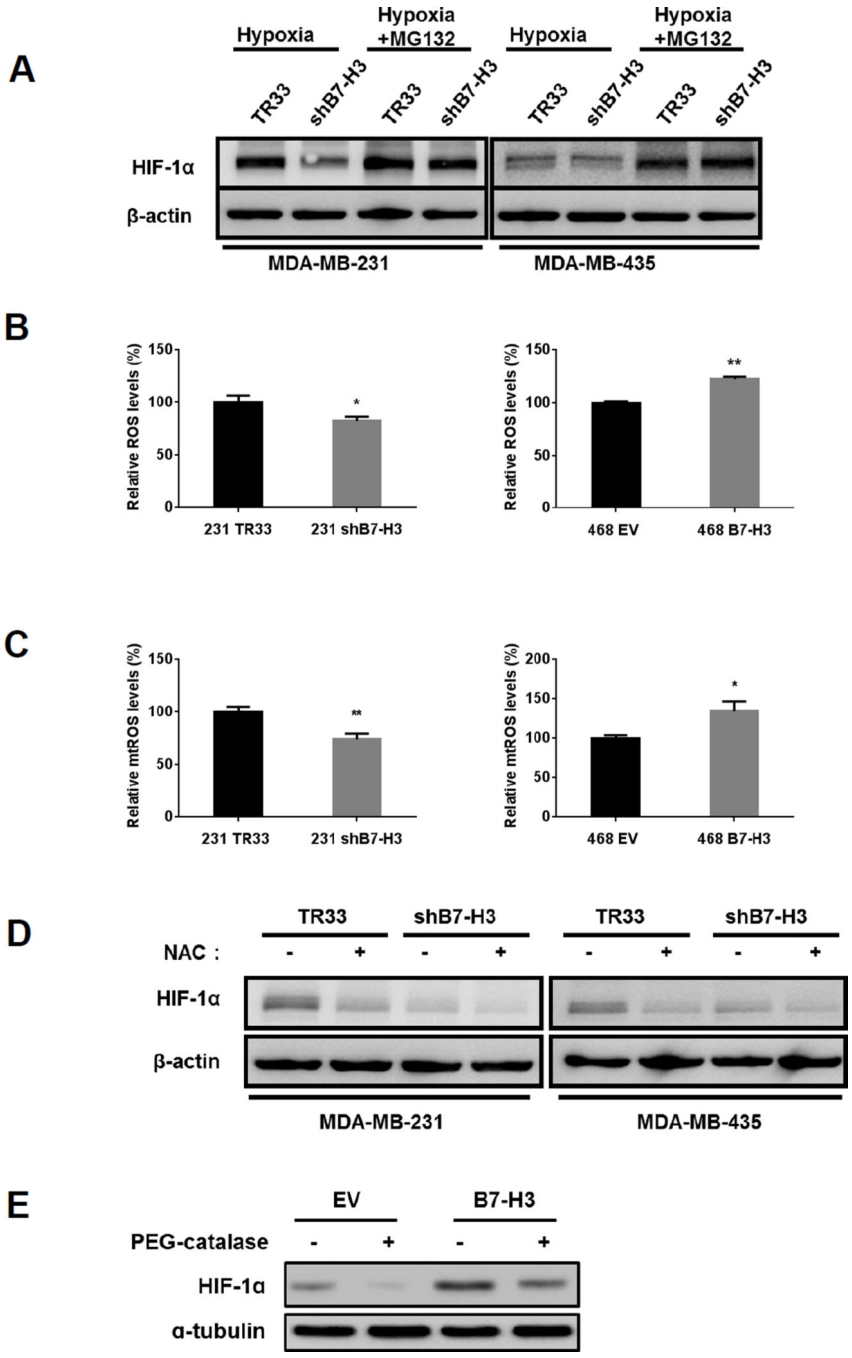

Figure 4. Reactive oxygen species (ROS) regulate HIF-1α protein stabilization induced by B7-H3

(A) MDA-MB-231 and MDA-MB-435 shB7-H3 knockdown cells grown under hypoxia conditions were incubated in the absence or presence of the proteasome inhibitor MG132 (20 μM for 1 hour) before harvesting cell lysates to determine HIF-1α protein levels by western-blotting. (B) MDA-MB-231 shB7-H3 knockdown and MDA-MB-468 B7-H3 overexpressing cells were grown in hypoxia for 48h and then trypsinized and labeled with CellROX to measure ROS levels by flow-cytometry. (±SE, three independent experiments; *p<0.05; **p<0.01). (C) MDA-MB-231 shB7-H3 and MDA-MB-468 B7-H3 cells were

grown in hypoxia for 48h and then trypsinized and labeled with MitoSOX to measure mitochondrial ROS levels by flow-cytometry. (±SE, three independent experiments; *p<0.05; **p<0.01). (D) MDA-MB-231 and MDA-MB-435 shB7-H3 knockdown cells grown under hypoxia conditions were incubated in the absence or presence of the ROS scavenger, N-acetyl-L-cysteine (NAC, 10mM for 24h) before harvesting cell lysates to determine HIF-1α protein levels by western-blotting. (E) MDA-MB-468 B7-H3 overexpressing cells grown under hypoxia conditions were incubated in absence or presence of PEG-catalase (500U/ml, pretreated for 1h before hypoxia) before harvesting cell lysates to determine HIF-1α protein levels by western-blotting.

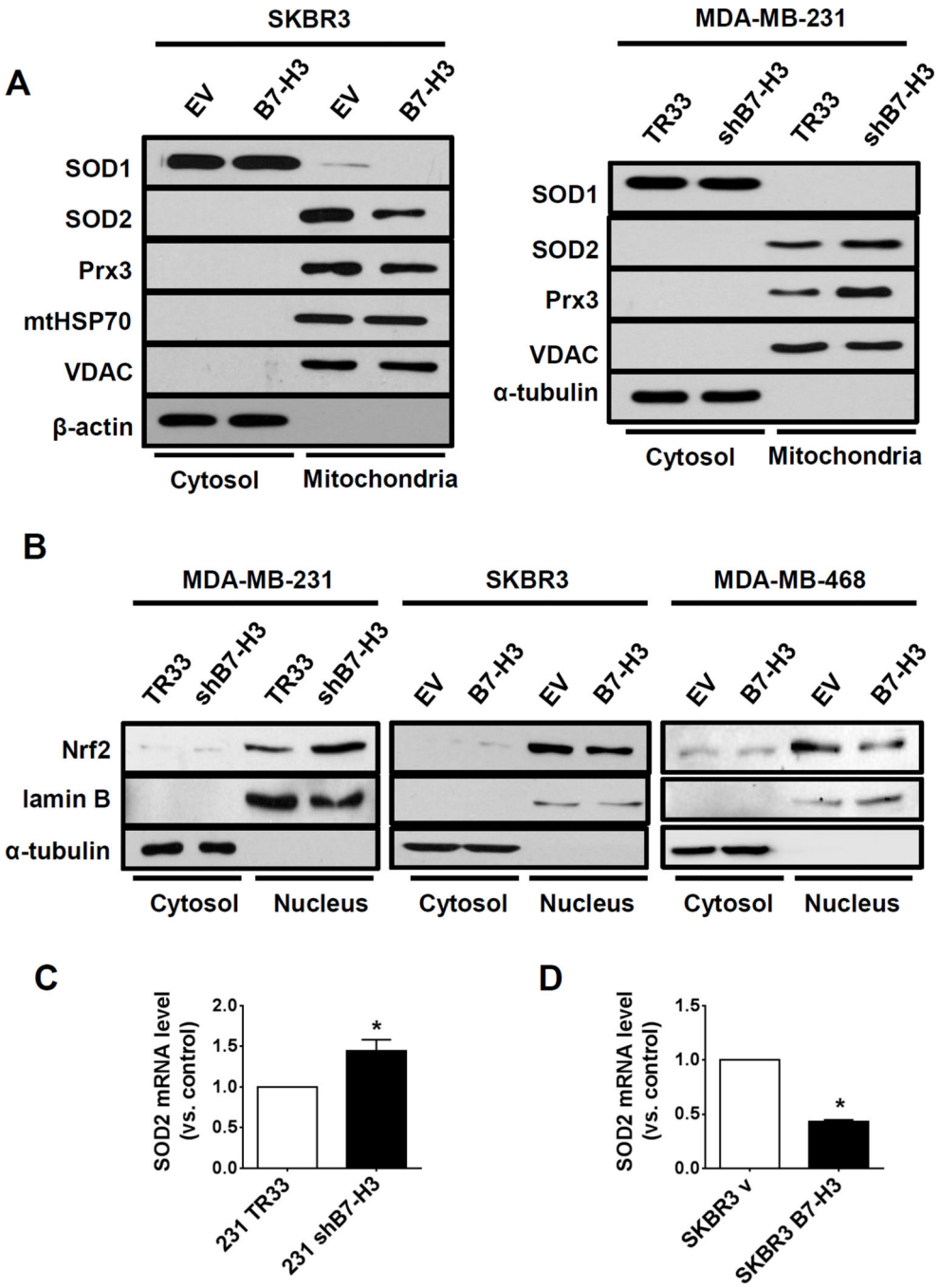

Figure 5. B7-H3 attenuates expression of mitochondrial antioxidant enzymes and suppresses Nrf2 nuclear translocation in breast cancer cells

(A) Antioxidant enzymes SOD1, SOD2 and PRX3 were measured by western-blotting of cytosolic and mitochondrial fractions of SKBR3 B7-H3 overexpressing cells (left panel) and MDA-MB-231 shB7-H3 knockdown cells (right panel). α-tubulin, mtHSP70 and VDAC were used as loading controls. (B) Nuclear translocation of Nrf2 was monitored by western-blotting of cytosolic and nuclear fractions of MDA-MB-231 shB7-H3 knockdown cells, SKBR3 B7-H3 and MDA-MB-468 B7-H3 overexpressing cells. Lamin B1 and α-tubulin were used as loading controls. (C–D) mRNA levels of SOD2 were measured by quantitative

RT-PCR in MDA-MB-231 shB7-H3 knockdown cells (C) and SKBR3 B7-H3 overexpression cells (D). Bar graphs represent average fold levels of measured mRNA (±SE, two independent experiments performed in triplicate, *$p<0.05$).

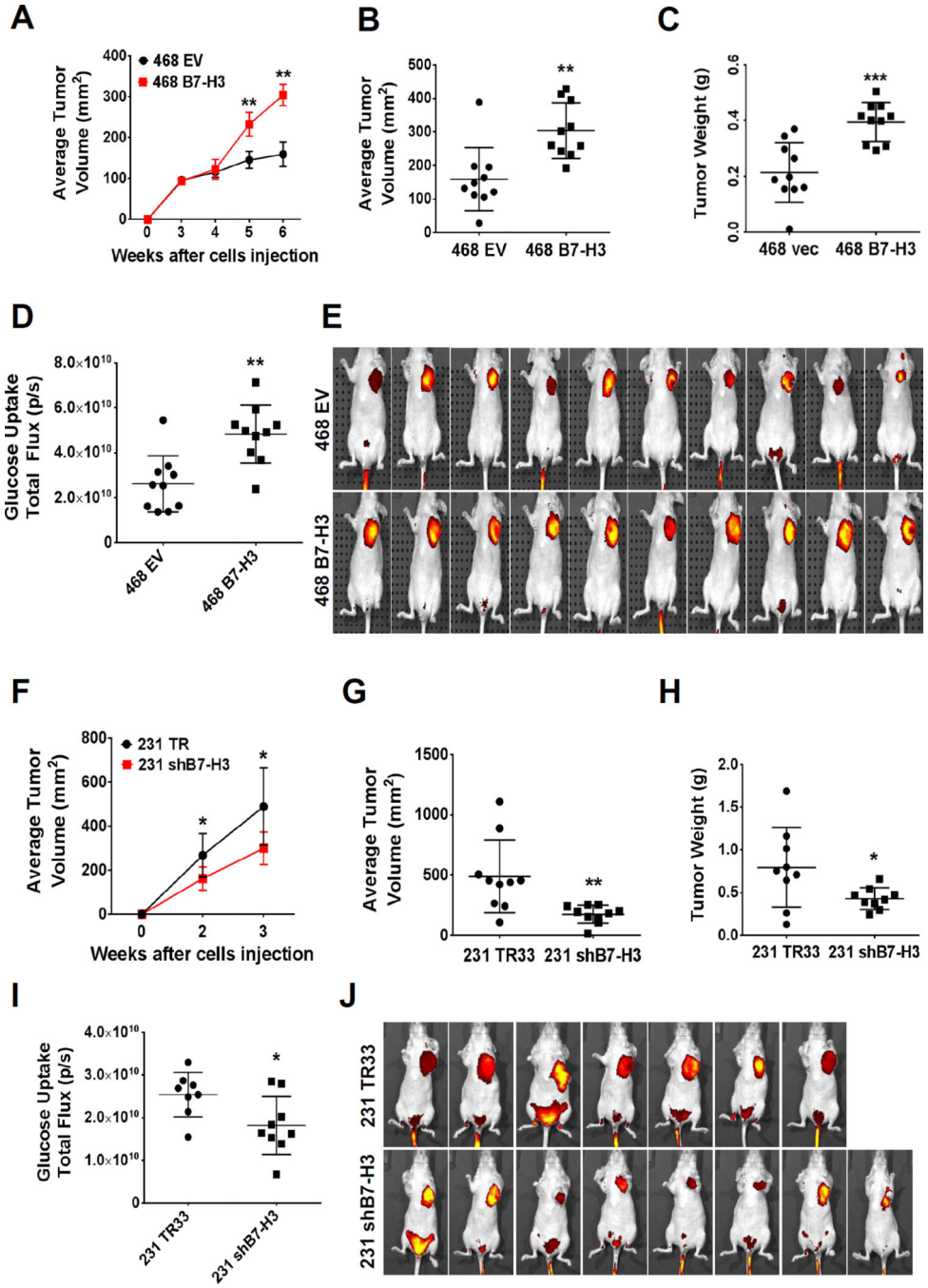

Figure 6. B7-H3 induces glucose uptake *in vivo* in breast cancer xenograft tumor studies

(A–E) MDA-MB-468 B7-H3 overexpressing breast cancer cells were implanted subcutaneously in athymic nude mice (EV, vector control cells) (n=10 mice/group). (A) Tumor volume was monitored by caliper measurements for 6 weeks post-injection (±SE, **p<0.0001). (B) Average tumor volume and (C) weight measured at 6 weeks post-injection (±SE, **p<0.005, ***p<0.001). (D–E) Glucose uptake was measured *in vivo* at 6 weeks post-injection of tumor cells using the fluorescent probe 2-DG-750, as described in Methods. (D) Average of total flux (photons/second) indicate intensity of 2-DG-750 uptake

at the primary site of cell injection around the mammary fatpad (±SE, **p<0.005; n=10 mice/group). (E) IVIS images of 2-DG-750 uptake in each individual mouse. (F–J) MDA-MB-231 shB7-H3 knockdown breast cancer cells were implanted subcutaneously in athymic nude mice (TR33, scramble control cells) (n=10 mice/group). (F) Tumor volume was monitored for 3 weeks after cell implantation (±SE, *p<0.01). (G) Average tumor volume (±SE, **p<0.005, n=10 mice/group) and (H) average tumor weight (±SE, *p<0.05, n=9 mice/group) measured at 3 weeks post-injection. (I–J) Glucose uptake was measured *in vivo* at 3 weeks post-injection of tumor cells using the fluorescent probe 2-DG-750, as described in Methods. (I) Average of total flux (photons/second) indicate intensity of 2-DG-750 uptake at the primary site of cell injection around the mammary fat pad (±SE, *p<0.005; n=7 mice/TR33 group and n=8 mice/shB7-H3 group). (E) IVIS images of 2-DG-750 uptake in each individual mouse. Excretory 2-DG-750 fluorescence signal was also visualized in the lower abdominal region near the bladder for several mice, as described by others (44); however, only the fluorescence signal at the primary site of the mammary xenograft tumors was considered for our analysis of total flux glucose uptake.

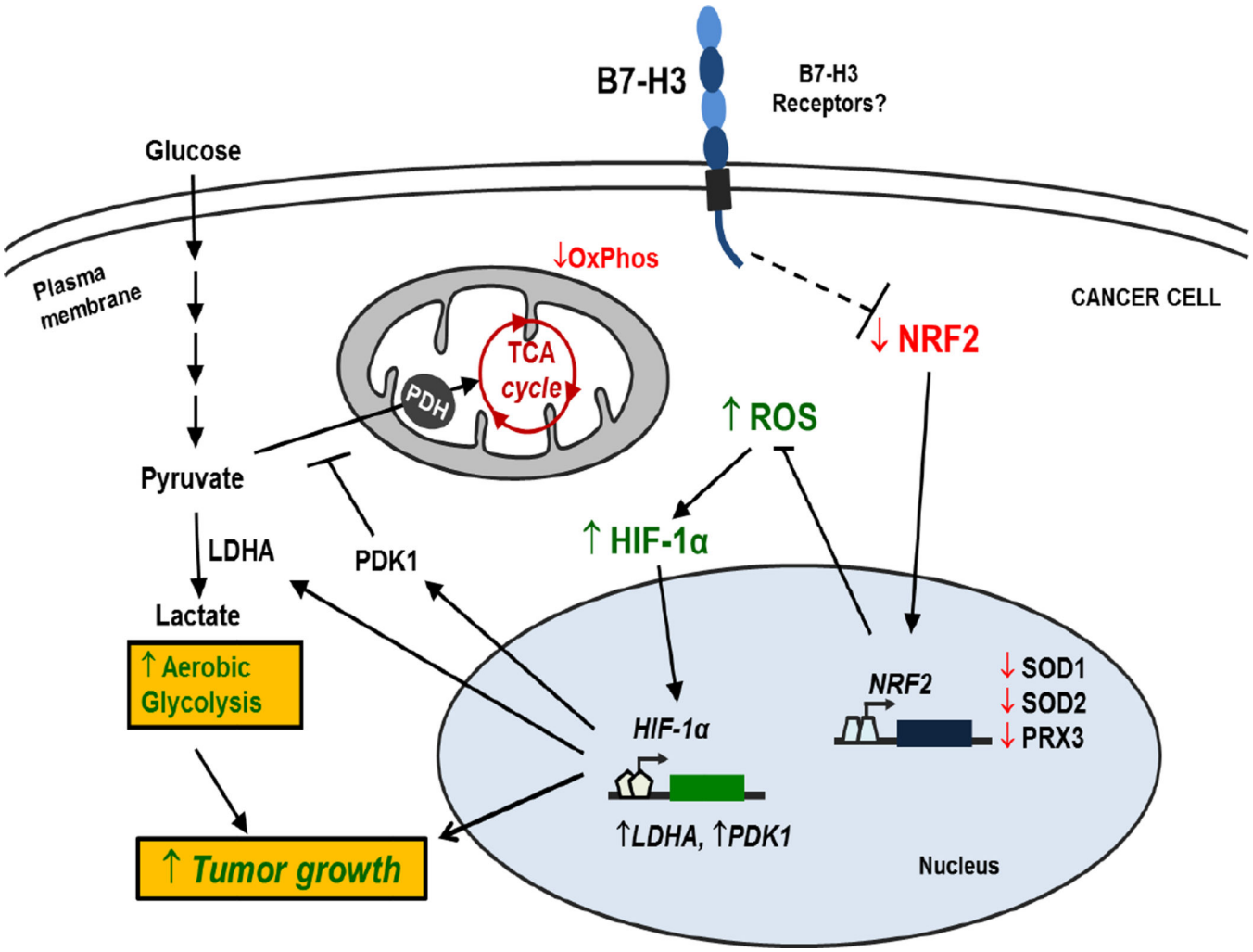

Figure 7. Model for the role of B7-H3 regulating glucose metabolism

Through unknown mechanisms, B7-H3 suppresses Nrf2 transcriptional activity, which in turn reduces transcription of the antioxidant enzymes SOD1, SOD2 and PRX3. As a result, B7-H3 overexpression leads to increased ROS in cancer cells. B7-H3-induced ROS stabilizes HIF-1α thus increasing the expression of glycolytic enzymes LDHA and PDK1, which promotes pyruvate conversion into lactate while inhibiting pyruvate flux through the TCA cycle. As a result, B7-H3 promotes aerobic glycolysis in cancer cells and therefore tumor growth.